Ninth International Conference on Computational Fluid Dynamics (ICCFD9), Istanbul, Turkey, July 11-15, 2016 **ICCFD9-229**

Numerical Simulation of Compressible Flow using Meshless Method Satisfying the Geometric Conservation Law

Jin Young Huh[1], Jae Sang Rhee[1], Kyu Hong Kim[2*] & Suk Young Jung[3]

[1] Department of Mechanical & Aerospace Engineering, Seoul National University, Seoul, Republic of Korea
[2] Department of Mechanical & Aerospace Engineering/Institute of Advanced Aerospace Technology, Seoul National University, Seoul, Republic of Korea
[3] Agency for Defense Development, Daejeon, Republic of Korea

Corresponding author: aerocfd1@snu.ac.kr

Abstract: A new Meshless method is developed to solve compressible flow with a strong shock wave robustly and accurately. By using the method of Lagrange multiplier, least squares method is applied with constraints which satisfy the geometric conservation law. The modified least squares method can improve robustness and accuracy of the Meshless method, compared with the original least squares method, especially when points are unevenly distributed. Numerical analyses of hypersonic flow over a blunt body with a strong shock wave were carried out using the developed Meshless method, then robustness, accuracy and convergence of their results were compared with those obtained from the original Least Squares Method and the Finite Volume Method.

Keywords: Meshless Method, Least Squares Method, Geometric Conservation Law, Lagrange multiplier.

1 Introduction

Generally, grid generation over complex geometry is known to be one of the primary difficulties in computational fluid dynamics. One method to solve this problem is Meshless method. Meshless method does not need rigid domain discretization which can usually be seen as grid form but only needs connectivity information of nodes. In this sense, the more difficult problems tackle, the more concerns of Meshless method arise. Many former researchers have studied until now and many Meshless methods have been developed. For example, there are Smooth Particle Hydrodynamics method, the Element Free Galerkin method, Hp-clouds method, the Reproducing Kernel Particle method and so on [1]. In compressible CFD field, Sridar's Upwind Finite Difference Scheme [2] and Katz's Moving Least Squares Method [3] are developed. Also, Huh [4] developed Meshless method for supersonic and hypersonic flow. However, the aforementioned methods have common weakness that excessive numerical oscillation can occur if points are not distributed in balance, which severely hinders accuracy and robustness.

In order to get over these shortcomings, the condition satisfying geometric conservation law is added to Meshless method. Also, AUSMPW+ scheme [5], which is originally developed for simulation of hypersonic flow at Finite Volume Method, is applied to the Meshless method to cure shock instability. A hypersonic blunt body problem was carried out as a validation case and the result of the developed method was compared with that of finite volume method.

2 Governing Equations

Consider the 3-D Euler equation in strong conservation law form

$$\frac{\partial q}{\partial t}+\frac{\partial f}{\partial x}+\frac{\partial g}{\partial y}+\frac{\partial h}{\partial z}=0 \tag{1}$$

where

$$q=\begin{bmatrix}\rho\\ \rho u\\ \rho v\\ \rho w\\ \rho E\end{bmatrix},\ f=\begin{bmatrix}\rho u\\ \rho u^2+P\\ \rho uv\\ \rho uw\\ \rho uH\end{bmatrix},\ g=\begin{bmatrix}\rho v\\ \rho vu\\ \rho v^2+P\\ \rho vw\\ \rho vH\end{bmatrix},\ h=\begin{bmatrix}\rho w\\ \rho wu\\ \rho wv\\ \rho w^2+P\\ \rho wH\end{bmatrix} \tag{2}$$

In Eq. (2), E means the total energy and H means the total enthalpy. For a calorically perfect gas, the equation of state is given by

$$E=\frac{P}{(\gamma-1)\rho}+\frac{1}{2}(u^2+v^2+w^2),\ H=E+\frac{P}{\rho} \tag{3}$$

with $\gamma=1.4$ for air.

3 Spatial Discretization

3.1. Taylor Series Least Squares Method

Least squares method [6,7,3] based on Taylor series expansions has been used to get unknown derivative terms of PDE represented on equation (1).
Ignoring high order terms, the Taylor expansion from the point cloud center (x_0,y_0,z_0) is shown as

$$\varphi(x,y)=\varphi_0+\Delta x\frac{\partial\varphi(x_0)}{\partial x}+\Delta y\frac{\partial\varphi(y_0)}{\partial y}+\Delta z\frac{\partial\varphi(z_0)}{\partial z}+O(\Delta^2) \tag{4}$$

Least squares problem with weighted function may be expressed as follow

$$min\sum_{j=1}^{m}\omega_j\left[\Delta\varphi_j-\Delta x_j\frac{\partial\varphi(x_0)}{\partial x}-\Delta y_j\frac{\partial\varphi(y_0)}{\partial y}-\Delta z_j\frac{\partial\varphi(z_0)}{\partial z}\right]^2 \tag{5}$$

$$\frac{\partial\varphi}{\partial x}\approx\sum_{j=1}^{m}a_j(\varphi_j-\varphi_0)=\sum_{j=1}^{m}a_j\Delta\varphi_j \tag{6}$$

$$\frac{\partial\varphi}{\partial y}\approx\sum_{j=1}^{m}b_j(\varphi_j-\varphi_0)=\sum_{j=1}^{m}b_j\Delta\varphi_j \tag{7}$$

$$\frac{\partial\varphi}{\partial z}\approx\sum_{j=1}^{m}c_j(\varphi_j-\varphi_0)=\sum_{j=1}^{m}\mathrm{c}_j\Delta\varphi_j \tag{8}$$

In equations above, m means the number of the point cloud of the center point. For a 3-D linear fit, the following equation can be obtained by solving Eq. (5).

$$AX=B \tag{9}$$

where

$$X^T=[a_j,b_j,c_j] \tag{10}$$

$$A = \begin{bmatrix} \Sigma\omega\Delta x^2 & \Sigma\omega\Delta x\Delta y & \Sigma\omega\Delta x\Delta z \\ \Sigma\omega\Delta x\Delta y & \Sigma\omega\Delta y^2 & \Sigma\omega\Delta y\Delta z \\ \Sigma\omega\Delta x\Delta z & \Sigma\omega\Delta y\Delta z & \Sigma\omega\Delta z^2 \end{bmatrix} \tag{11}$$

$$B^T = [\omega_j \Delta x_j, \omega_j \Delta y_j, \omega_j \Delta z_j] \tag{12}$$

Solving the matrix equation in Eq. (9), explicit formulas of the least squares method coefficients are calculated as follow

$$a_j = \frac{M_{11}}{|A|}\omega_j \Delta x_j + \frac{M_{12}}{|A|}\omega_j \Delta y_j + \frac{M_{13}}{|A|}\omega_j \Delta z_j \tag{13}$$

$$b_j = \frac{M_{21}}{|A|}\omega_j \Delta x_j + \frac{M_{22}}{|A|}\omega_j \Delta y_j + \frac{M_{23}}{|A|}\omega_j \Delta z_j \tag{14}$$

$$c_j = \frac{M_{31}}{|A|}\omega_j \Delta x_j + \frac{M_{32}}{|A|}\omega_j \Delta y_j + \frac{M_{33}}{|A|}\omega_j \Delta z_j \tag{15}$$

where

$$\begin{aligned} |A| = \sum \omega\Delta x^2 \sum \omega\Delta y^2 \sum \omega\, \Delta z^2 \left[1 - \frac{(\sum \omega\Delta x\Delta z)^2}{\sum \omega\Delta x^2 \sum \omega\Delta z^2} - \frac{(\sum \omega\Delta x\Delta y)^2}{\sum \omega\Delta x^2 \sum \omega\Delta y^2} \right. \\ \left. - \frac{(\sum \omega\Delta y\Delta z)^2}{\sum \omega\Delta y^2 \sum \omega\Delta z^2}\right] + 2[\sum \omega\Delta x\Delta y \sum \omega\Delta y\Delta z \sum \omega\Delta x\Delta z] \end{aligned} \tag{16}$$

$$M_{11} = \sum \omega\Delta y^2 \sum \omega\Delta z^2 - \left(\sum \omega\Delta y\Delta z\right)^2 \tag{17}$$

$$M_{12} = M_{21} = \sum \omega\Delta x\Delta z \sum \omega\Delta y\Delta z - \sum \omega\Delta x\Delta y \sum \omega\Delta z^2 \tag{18}$$

$$M_{13} = M_{31} = \sum \omega\Delta x\Delta y \sum \omega\Delta y\Delta z - \sum \omega\Delta x\Delta z \sum \omega\Delta y^2 \tag{19}$$

$$M_{22} = \sum \omega\Delta x^2 \sum \omega\Delta z^2 - \left(\sum \omega\Delta x\Delta z\right)^2 \tag{20}$$

$$M_{23} = M_{32} = \sum \omega\Delta x\Delta z \sum \omega\Delta x\Delta y - \sum \omega\Delta y\Delta z \sum \omega\Delta x^2 \tag{21}$$

$$M_{33} = \sum \omega\Delta x^2 \sum \omega\Delta y^2 - \left(\sum \omega\Delta x\Delta y\right)^2 \tag{22}$$

Simply, an inverse distance form can be chosen as the weighting function shown as follows.

$$\omega_j = \frac{1}{(\Delta x_j^2 + \Delta y_j^2 + \Delta z_j^2)^{1/2}} \tag{23}$$

3.2. Proposed Method: Least Squares Method with Geometric Conservation Law (GC-LSM)

The coefficients of a Meshless method satisfy conservation law, if the coefficients satisfy following two conditions.
Geometric conservation law and 1st order consistency:

$$\begin{gathered}
\sum_{j=1}^{m} a_{ij} = 0,\ \sum_{j=1}^{m} b_{ij} = 0,\ \sum_{j=1}^{m} c_{ij} = 0 \\
\sum_{j=1}^{m} a_{ij}x_j = 1, \quad \sum_{j=1}^{m} b_{ij}x_j = 0, \quad \sum_{j=1}^{m} c_{ij}x_j = 0 \\
\sum_{j=1}^{m} a_{ij}x_j = 0, \quad \sum_{j=1}^{m} b_{ij}x_j = 1, \quad \sum_{j=1}^{m} c_{ij}x_j = 0 \\
\sum_{j=1}^{m} a_{ij}x_j = 0, \quad \sum_{j=1}^{m} b_{ij}x_j = 0, \quad \sum_{j=1}^{m} c_{ij}x_j = 1
\end{gathered} \tag{24}$$

Flux conservation law:

$$a_{ij} = -a_{ji},\ b_{ij} = -b_{ji},\ c_{ij} = -c_{ji} \tag{25}$$

Geometric conservation law prevents self creation or diminution of physical quantities like mass, momentum, or energy in a cell. If the value of the point is local extrema, geometric conservation condition inhibits divergence of the value. Because closed geometry like grid system satisfies condition of 1st order consistnecy, it should be also considered with geometric conservation. On the other hand, flux conservation law keeps the rule that the influx and outflux between connected nodes are the same. As described below in Eq.(26 – 30), the least squares method with the constraints, which are geometric conservation law and 1st order consistency, could be solved by calculating the matrix equation whose size is (3m+12) × (3m+12) when m is the number of the connectivity of the node. However, if flux conservation law is added to the constraints, the size of the matrix to solve least squares problem might be (4.5nm+12n) × (4.5nm+12n) when n is the number of all nodes in the numerical domain. Its matrix size is so large in 3-D practical problems including multi-body or movement that solving the problem may seem to be unrealistic. Moreover, exclusion of the flux conservation law couldn't show dramatic performance deficiency in the present validation cases. So we propose the least squares method with only geometric conservation law and 1st order consistency. Although this method cannot satisfy conservation law rigorously, it shows value in use of CFD about practical problems through improvements of the accuracy and robustness in compressible flows and fast computation to get least squares coefficients.

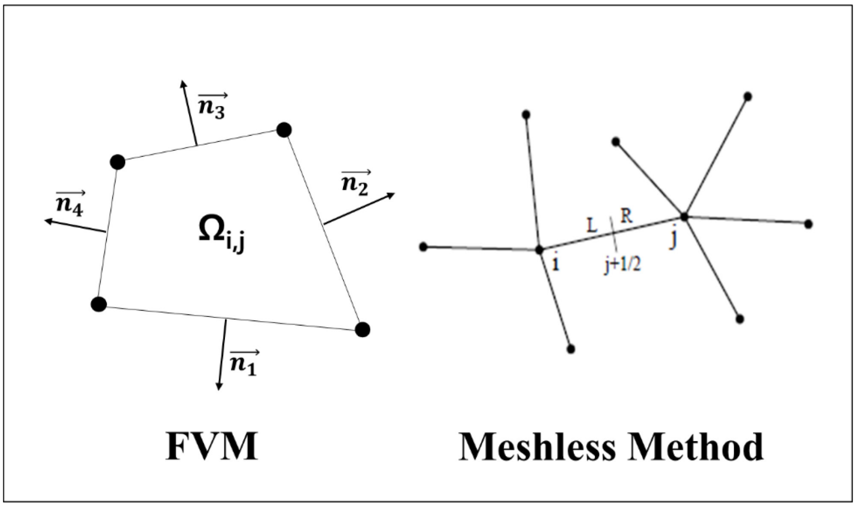

Figure 1: Comparison of geometry of FVM and Meshless method

In this study, the method of Lagrange multiplier was used to find minima of eq. (5) with the constraints expressed as eq. (24). The Lagrange function can be defined as

$$\Lambda \equiv F_i + \sum_{p=1}^{3} \mu_p M_{p,i} + \sum_{p=1}^{3}\sum_{l=1}^{3} \nu_{p,l} N_{p,l,i} \tag{26}$$

where F is an objective function, and M and N are constraints as follow.

$$F_i = \sum_{j=1}^{m} \omega_{ij} \left[\Delta\varphi_{ij} - \Delta x_{ij} \left(\sum_{k=1}^{m} a_{ik} \Delta\phi_{ik} \right) - \Delta y_{ij} \left(\sum_{k=1}^{m} b_{ik} \Delta\phi_{ik} \right) - \Delta z_{ij} \left(\sum_{k=1}^{m} c_{ik} \Delta\phi_{ik} \right) \right]^2 \tag{27}$$

$$\begin{gathered}
M_{1,i} = \sum_{j=1}^{m} a_{ij} = 0, \quad M_{2,i} = \sum_{j=1}^{m} b_{ij} = 0, \quad M_{3,i} = \sum_{j=1}^{m} c_{ij} = 0 \\
N_{1,1,i} = \sum_{j=1}^{m} a_{ij} x_j = 1, \quad N_{1,2,i} = \sum_{j=1}^{m} b_{ij} x_j = 0, \quad N_{1,3,i} = \sum_{j=1}^{m} c_{ij} x_j = 0 \\
N_{2,1,i} = \sum_{j=1}^{m} a_{ij} x_j = 0, \quad N_{2,2,i} = \sum_{j=1}^{m} b_{ij} x_j = 1, \quad N_{2,3,i} = \sum_{j=1}^{m} c_{ij} x_j = 0 \\
N_{3,1,i} = \sum_{j=1}^{m} a_{ij} x_j = 0, \quad N_{3,2,i} = \sum_{j=1}^{m} b_{ij} x_j = 0, \quad N_{3,3,i} = \sum_{j=1}^{m} c_{ij} x_j = 1
\end{gathered} \tag{28}$$

where M means geometric conservation law and N means 1st order consistency. To get the constrained extrema of F_i, we just solve $\nabla\Lambda = 0$, then finally we can get the simple matrix equation as follow.

$$\mathrm{AX} = \mathrm{B} \tag{29}$$

where

$$\mathrm{A} = \begin{bmatrix} D & E \\ E^T & 0 \end{bmatrix},$$

$$\mathrm{D} = \begin{bmatrix} d_1 & & 0 \\ & \ddots & \\ 0 & & d_n \end{bmatrix}_{3\mathrm{m} \times 3m},$$

$$d_i = \begin{bmatrix} \sum_{k=1}^{m} \omega_{ik} \Delta x_{ik}^2 & \sum_{k=1}^{m} \omega_{ik} \Delta x_{ik} \Delta y_{ik} & \sum_{k=1}^{m} \omega_{ik} \Delta x_{ik} \Delta z_{ik} \\ \sum_{k=1}^{m} \omega_{ik} \Delta x_{ik} \Delta y_{ik} & \sum_{k=1}^{m} \omega_{ik} \Delta y_{ik}^2 & \sum_{k=1}^{m} \omega_{ik} \Delta y_{ik} \Delta z_{ik} \\ \sum_{k=1}^{m} \omega_{ik} \Delta x_{ik} \Delta z_{ik} & \sum_{k=1}^{m} \omega_{ik} \Delta y_{ik} \Delta z_{ik} & \sum_{k=1}^{m} \omega_{ik} \Delta z_{ik}^2 \end{bmatrix}, \tag{30}$$

$$E = \begin{bmatrix} e_3 \\ \vdots \\ e_3 \end{bmatrix}_{3m \times 12}, e_3 = \begin{bmatrix} 1 & 0 & 0 & x & 0 & 0 & y & 0 & 0 & z & 0 & 0 \\ 0 & 1 & 0 & 0 & x & 0 & 0 & y & 0 & 0 & z & 0 \\ 0 & 0 & 1 & 0 & 0 & x & 0 & 0 & y & 0 & 0 & z \end{bmatrix}$$

$$X^T = [a_{i1}, b_{i1}, c_{i1}, \dots, a_{im}, b_{im}, c_{im}, \mu_1, \mu_2, \mu_3, \nu_{1,1}, \nu_{1,2}, \dots, \nu_{3,3}],$$

$$B^T = [\omega_{i1}\Delta x_{i1}, \omega_{i1}\Delta y_{i1}, \omega_{i1}\Delta z_{i1}, \dots, \omega_{im}\Delta x_{im}, \omega_{im}\Delta y_{im}, \omega_{im}\Delta z_{im}, 0,0,0,1,0,0,0,1,0,0,0,1]$$

In this study, LU-decomposition was used to solve matrix inversion.

3.3. A method for the accurate computations in hypersonic flows: AUSMPW+ scheme

Using the above algorithm, the discretization form of the governing equations at point i results in

$$\frac{\partial q_i}{\partial t} + \sum_{j=1}^{m} a_{ij}\Delta f_{ij} + \sum_{j=1}^{m} b_{ij}\Delta g_{ij} + \sum_{j=1}^{m} c_{ij}\Delta h_{ij} = 0 \tag{31}$$

Eq. (31) represents a non-dissipative, unstable discretization [3]. To get stabilization, the mid-point flux at $ij + 1/2$ which is the middle of the edge connecting nodes i and j is introduced, as shown in Fig. (2). So, Eq. (31) can be modified as follow,

$$\frac{\partial q_i}{\partial t} + 2\sum_{j=1}^{m} a_{ij}(f_{ij+1/2} - f_i) + 2\sum_{j=1}^{m} b_{ij}(g_{ij+1/2} - g_i) + 2\sum_{j=1}^{m} c_{ij}(h_{ij+1/2} - h_i) = 0 \tag{32}$$

For the accurate and stable computations in hypersonic flow region, ASUMPW+ scheme [5] may be used to find the mid-point flux..

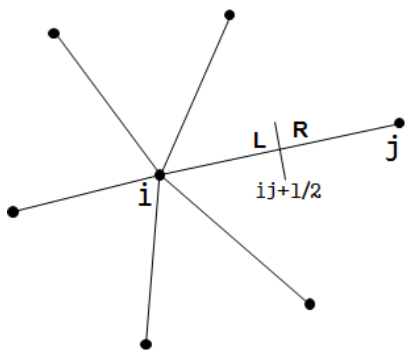

Figure 2: Illustration of mid-point on the edge connecting nodes i and j

AUSMPW+ is originally developed in finite volume method to increase the accuracy and computational efficiency in capturing an oblique shock without compromising robustness.
The numerical flux of AUSMPW+ can be obtained as follows.

$$f_{ij+1/2} = \bar{M}^{+}{}_{L} c_{\frac{1}{2}} \Phi_L + \bar{M}^{-}{}_{R} c_{\frac{1}{2}} \Phi_R + (P_L^{+} P_L + P_R^{-} P_R) \tag{33}$$

$\Phi = (\rho, \rho u, \rho v, \rho w, \rho H)^T$ *and* $P = (0, a_{ij}\, p, b_{ij} p, c_{ij} p, 0)^T$. *The* subscripts 1/2 and (L,R) stand for a quantity at a midpoint on the edge of Fig. 2 and the left and right states across the edge, respectively. The Mach number at midpoint is defined as

$$m_{\frac{1}{2}} = M_L^{+} + M_R^{-} \tag{34}$$

when $\overline{M_L^{+}}$ and $\overline{M_R^{-}}$ are given as follows.
If $m_{\frac{1}{2}} = M_L^{+} + M_R^{-} \geq 0$, then

$$\overline{M_L^{+}} = M_L^{+} + M_R^{-}[(1-w)(1+f_R) - f_L] \tag{35}$$

$$\overline{M_R^{-}} = M_R^{-} w(1+f_R) \tag{36}$$

If $m_{\frac{1}{2}} = M_L^{+} + M_R^{-} < 0$, then

$$\overline{M_L^{+}} = M_L^{+} + w(1+f_L) \tag{37}$$

$$\overline{M_R^-} = M_R^- + M_L^+[(1-w)(1+f_L) - f_R] \tag{38}$$

with

$$w(P_L, P_R) = 1 - min\left(\frac{P_L}{P_R}, \frac{P_R}{P_L}\right)^3 \tag{39}$$

The pressure-based weight function is simplified to

$$f_{L,R} = \left(\frac{P_{L,R}}{P_s} - 1\right), P_s \neq 0 \tag{40}$$

where

$$P_s = P_L^+ P_L + P_R^- P_R \tag{41}$$

The split Mach number is defined by

$$M^\pm = \begin{cases} \pm\frac{1}{4}(M \pm 1)^2, & |M| \leq 1 \\ \frac{1}{2}(M \pm |M|), & |M| > 1 \end{cases} \tag{42}$$

$$P^\pm = \begin{cases} \frac{1}{4}(M \pm 1)^2(2 \mp M), & |M| \leq 1 \\ \frac{1}{2}(1 \pm sign(M)), & |M| > 1 \end{cases} \tag{43}$$

The Mach number of each side is

$$M_{L,R} = \frac{U_{L,R}}{c_{s,1/2}} \tag{44}$$

and the speed of sound($c_{1/2}$) is

$$c_{s,1/2} = \begin{cases} min\left(\frac{c_s^{*2}}{max(|U_L|, c_s^*)}\right), \frac{1}{2}(U_L + U_R) > 0 \\ min\left(\frac{c_s^{*2}}{max(|U_R|, c_s^*)}\right), \frac{1}{2}(U_L + U_R) < 0 \end{cases} \tag{45}$$

where

$$c_s^* = \sqrt{2(\gamma - 1)/(\gamma + 1)H_{normal}} \tag{46}$$

$$H_{normal} = \frac{1}{2}(H_L - \frac{1}{2}V_L^2 + H_R - \frac{1}{2}V_R^2) \tag{47}$$

3.4. Spatial Reconstruction Scheme: Minmod Limiter

No reconstruction scheme such that $\Phi_L = \Phi_i, \Phi_R = \Phi_j$ have first-order spatial accuracy in general. To improve accuracy, TVD scheme is adopted to the Meshless method. In this study, minmod limiter [4] is used to reconstruct the solution to the mid-point of each edge. The basic form of spatial interpolation is given by

$$\begin{aligned} \Phi_L &= \Phi_i + 0.5 * \phi_L * (\Phi_j - \Phi_i) \\ \Phi_R &= \Phi_j + 0.5 * \phi_R * (\Phi_i - \Phi_j) \end{aligned} \tag{48}$$

In order to apply to Meshless method, it is necessary to modify minmod limiter as follows. In Meshless method, ϕ is given by

$$\phi = max(0, min(1, r_k)), \tag{49}$$

where $k \in \{local\ point\ cloud\ of\ node\ i\ \&\ \theta_{kij}\ is\ max\}$,

$$r_k = \frac{s_{ik'}}{s_{ji}} = \frac{s_{ki}}{s_{ji}} cos(\theta_{kij}), \tag{50}$$

$$s_{ki} = \frac{\Phi_k - \Phi_i}{\|\vec{x_k} - \vec{x_i}\|} \tag{51}$$

Since there is no point on the opposite side of point j in the vicinity of point i in general point system, nearest point k to the opposite side is used to calculate r_k shown in Fig. 3.

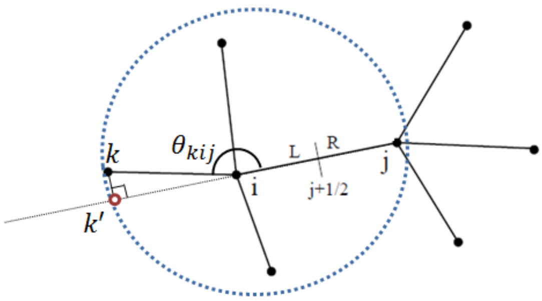

Figure 3: Minmod limiter for Meshless method

4 Temporal Integration

Applying Eq. (32) to each node, the result is obtained in the following form.

$$\frac{\partial q_i}{\partial t} + 2\sum_{j=1}^{m}(F_{ij} - F_i) = 0 \tag{52}$$

where flux $F = af + bg + ch$ which is similar to a directional flux through a face area on an mesh in FVM. The Eq. (52) can be integrated either by explicit or implicit methods.

4.1. Explicit Time Integration: Runge-Kutta Method

Eq. (52) can be presented in an explicit form as follows.

$$\frac{\partial q_i^{n+1}}{\partial t} + \mathrm{R}(q_i^n) = 0 \tag{53}$$

where R is represented by

$$\mathrm{R}(q_i) = 2\sum_{j=1}^{m}(F_{ij} - F_i) \tag{54}$$

In this study, the four-stage Runge-Kutta method is used as follows [8].

$$\begin{aligned} q^{(0)} &= q^{(n)} \\ q^{(1)} &= q^{(0)} - \alpha_1 \Delta t \mathrm{R}(q^{(0)}) \\ &\vdots \\ q^{(4)} &= q^{(0)} - \alpha_4 \Delta t \mathrm{R}(q^{(3)}) \end{aligned} \tag{55}$$

$$q^{(n+1)} = q^{(4)}$$

4.2. Implicit Time Integration: LU-SGS Method

Referring to the works of Yoon [9] and Chen [10], LU-SGS is adopted to Meshless Method. By applying Eq. (52), the governing equations written in discrete form as Eq. (52) can be integrated in time using a fully implicit time discretization as follows.

$$\frac{\partial q_i^{n+1}}{\partial t} + R_i^{n+1} = \frac{\partial q_i^{n+1}}{\partial t} + 2\sum_j^m \left(F_{ij}^{n+1} - F_i^{n+1}\right) = 0 \tag{56}$$

The flux function, F_{ij}^{n+1} may be linearized as

$$F_{ij}^{n+1}(q_i, q_j) \approx F_{ij}^n + A_{ij}^+(q_i)\delta q_i + A_{ij}^-(q_j)\delta q_j \tag{57}$$

where matrices $A_{ij}^{\pm}$ are constructed as

$$A_{ij}^{\pm} = \frac{1}{2}(A_{ij} \pm \lambda_{ij} I) \tag{58}$$

where A_{ij} and I is Jacobian matrix and the identity matrix, and $\lambda_{ij} \geq \max(|\lambda_A|)$. Here, λ_A represents eigenvalues of Jacobian matrix. Then Eq. (56) can be integrated as

$$\left(\frac{1}{\Delta t_i} + \sum_j^m \lambda_{ij}\right)\delta q_i + 2\sum_{j \in LC} A_{ij}^- \delta q_j + 2\sum_{j \in UC} A_{ij}^- \delta q_j - \sum_j^m A_{ij}\delta q_i = -R_i^n \tag{59}$$

where Δt_i is local time step and subset LC and UC are defined as follows.

$$\begin{aligned} &LC(Lower\ Cloud) \equiv \{j |\, j < i \,\&\, j \in S_i\} \\ &UC(Upper\ Cloud) \equiv \{j |\, j > i \,\&\, j \in S_i\} \end{aligned} \tag{60}$$

The set, S_i is the local point cloud at node i. From Eq. (24), the sum of the Jacobian matrix A_{ij} should be zero. Thus, Eq. (59) can be written in LU-SGS form as

$$LD^{-1}U\delta q_i = -R_i^n \tag{61}$$

where

$$\begin{aligned} D &= \left(\frac{1}{\Delta t} + \sum_j^m \lambda_{ij}\right) I \\ L &= \left(\frac{1}{\Delta t} + \sum_j^m \lambda_{ij}\right) I + 2\sum_{j \in LC} A_{ij}^- \frac{\delta q_j}{\delta q_i} \\ U &= \left(\frac{1}{\Delta t} + \sum_j^m \lambda_{ij}\right) I + 2\sum_{j \in UC} A_{ij}^- \frac{\delta q_j}{\delta q_i} \end{aligned} \tag{62}$$

4.3. Local Time Stepping

Local time stepping at any node i may be calculated for steady flows.

$$\Delta t_i = \frac{CFL}{\sum_{j=1}^m \left(\left|a_{ij}u + b_{ij}v + c_{ij}w\right| + c_s\sqrt{a_{ij}^2 + b_{ij}^2 + c_{ij}^2}\right)} \tag{63}$$

where $a_{ij}, b_{ij}, and\ c_{ij}$ are least squares coefficients.

5 Numerical Results

5.1. Sine Wave

To investigate the spatial accuracy of the developed scheme, a fundamental grid convergence study was performed. A 2-D periodic sine wave problem whose analytical exact gradient is easily found was selected to compare the computed results with the exact solution. The initial profile of the wave is given as follows.

$$\rho = 1 + 0.2\sin(8\pi(x_0 - x)) \tag{64}$$

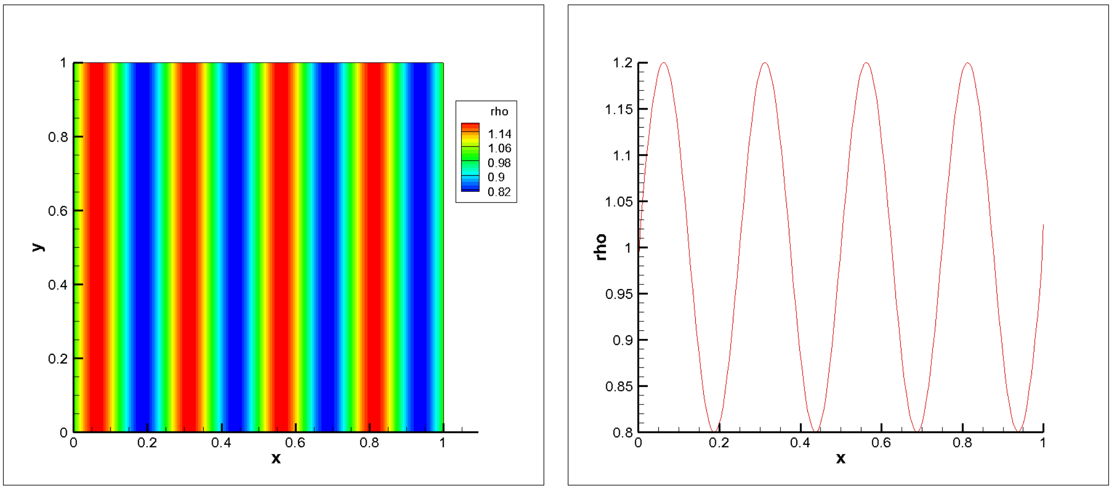

Figure 4: Initial profile

The speed of the wave is 0.1, and the grid systems used is shown in Fig. (5). Regular grid (or square grid) has two sets of lines perpendicular to each other, and random grid are computed as follows.

$$\begin{aligned} x_{random} &= x_{regular} + \kappa \cdot d_x \cdot RN_x \\ y_{random} &= y_{regular} + \kappa \cdot d_y \cdot RN_y \end{aligned} \tag{65}$$

where κ, d, and RN are each random grid coefficient, grid interval, and random number which is a randomly chosen number between 0 and 1. In this study, the value of κ is 0.75. The nodes for Meshless analysis are obtained from the grid, and the nearest 8-points at any node before grid distortion are selected as the connectivity of the node. The mid-point flux scheme is AUSMPW+, and the boundary conditions are periodic conditions. The 4th order Runge-Kutta method with $\Delta t = 0.0001$ was used for time integration. Three methods(Least Squares Method, Least Squares Method with Geometric Conservation Law, Finite Volume Method) are tested with four different grid sizes($51 \times 51, 101 \times 101, 201 \times 201, 401 \times 401$). Fig. (6) shows the results at t=1s.
The result of the original Least Squares Method may diverge with excessive numerical oscillation on the random grid. On the contrary, the proposed method can cure the unphysical oscillation and it is possible to obtain a converged solution on random grid. The L_2-norm of the error between the exact and numerical results is compared at t=1 s. Shown in Table (1), the GC-LSM does not lose accuracy compared to the result on regular grid, although the others, in addition to most other well-known linear preserving schemes, lose order of accuracy as a grid become distorted. Moreover, though the proposed method even does not satisfy flux conservation law, non-conservative feature is not found.

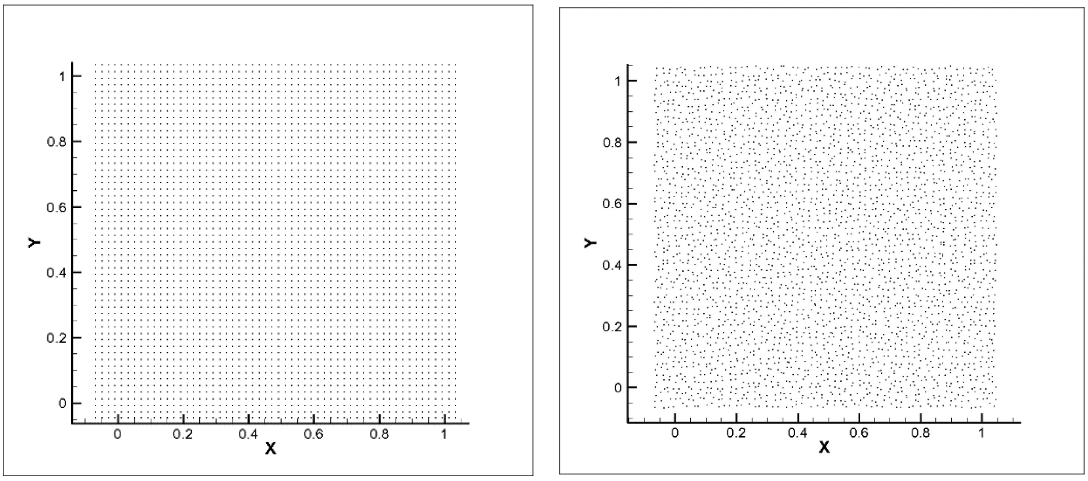

Figure 6: Regular grid and random grid

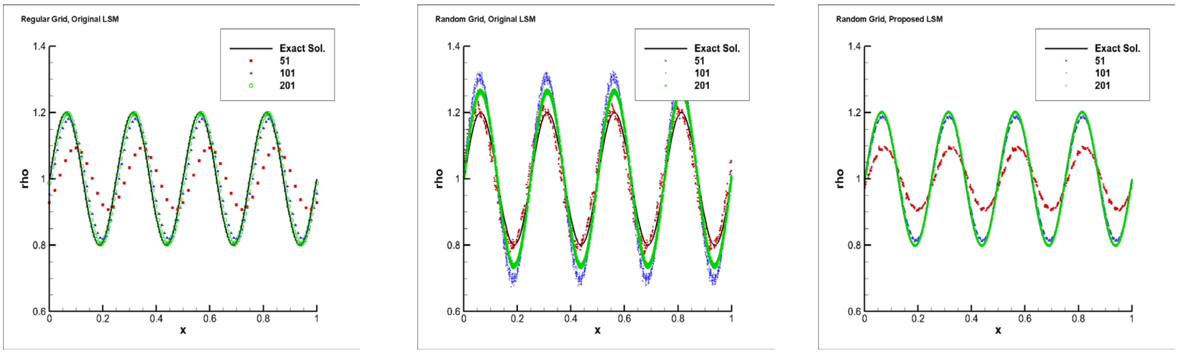

(a) (b) (c)

Figure 5: Results of the sine wave problem : (a) FVM on regular grid, (b) LSM on random grid, (c) GC-LSM on random grid

Table 1: Grid refinement test for the advection of the sine wave problem

		Grid	L^2	Order
Original LSM	Regular Grid	51x51	6.1043E-02	-
		101x101	1.7713E-02	1.785
		201x201	4.5605E-03	1.958
	Random Grid	51x51	1.5394E-02	-
		101x101	3.0832E-02	-1.002
		201x201	1.9697E-02	0.646
GC-LSM	Regular Grid	51x51	6.1043E-02	-
		101x101	1.7713E-02	1.785
		201x201	4.5605E-03	1.958
	Random Grid	51x51	4.3327E-02	-
		101x101	7.5052E-03	2.529
		201x201	1.6536E-03	2.182

5.2. Hypersonic Blunt Body

The second validation case is a blunt body problem in hypersonic flows. Its purpose is to check the robustness, accuracy, convergence of the developed method. The free stream Mach number, M_{∞}, is 10, so a strong shock wave appear in front of the blunt body. Two types of the grid are used for this test. One of them is a balanced grid and the other is a perturbed grid, as shown in Fig. (7). The latter can be constructed by Eq. (65) in a similar way. So, the computing nodes and the connectivity are chosen in the same manner as the first validation case. AUSMPW+ scheme and LU-SGS scheme were used for the mid-point flux and time integration method, respectively. To remove the numerical oscillation around shock wave, Minmod limiter was used.

Fig. (8) shows pressure distribution of Least Squares Method, Least Squares Method with Geometric Conservation Law and Finite Volume Method on the perturbed grid. The result of the FVM on balanced grid ($\boldsymbol{\kappa} = \mathbf{0.0}$) is a reference of the case. The pressure distribution along stagnation line shown in Fig. (8) indicates that the proposed method has better shock capturing performance such as shock position and strength, compared to original LSM. Also, we can see that only satisfaction of the geometric conservation law without flux conservation law can effectively enhances accuracy and robustness of the solution. The convergence histories (L^2-norm error) presented in Fig. (9) show that the proposed method also converged to machine accuracy. Thus, the proposed method is recommended for simulation of compressible flows, especially for hypersonic flows.

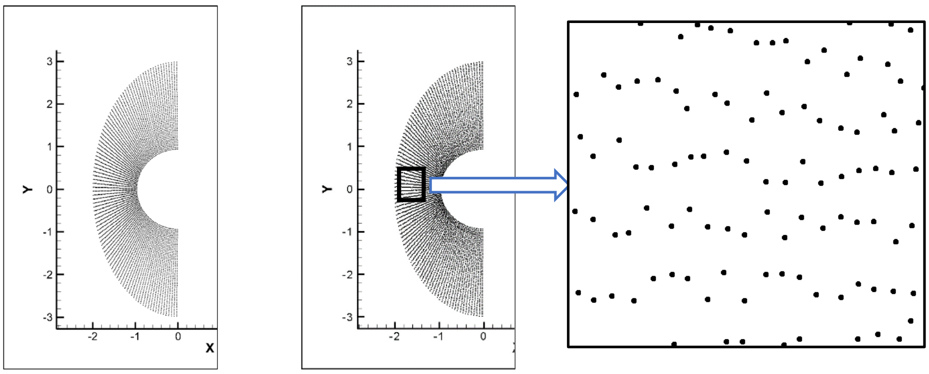

Figure 7: balanced grid and perturbed grid($\boldsymbol{\kappa} = \mathbf{0.5}$)

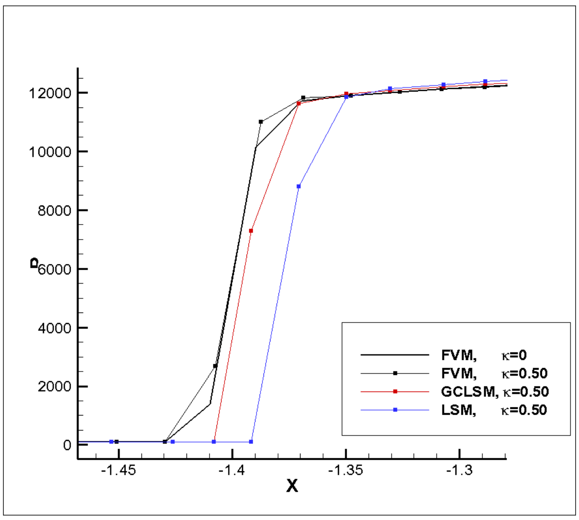

Figure 8: pressure distribution along stagnation line ($\boldsymbol{\kappa} = \mathbf{0.5}$)

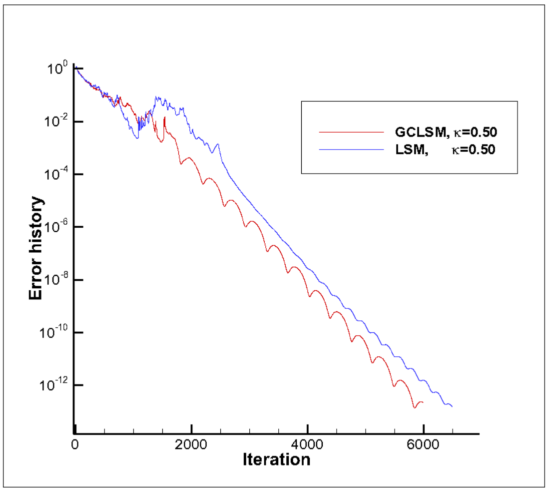

Figure 9: Comparisons of convergence histories

5.3. Moving Sphere

A moving sphere problem was selected as the last validation case. This problem was chosen to verify the accuracy and robustness in more complex grid system. The node distribution is shown in Fig. (10), and total number of nodes is 722,464. The nodes and connectivity generation algorithm which is developed by Rhee [11] are used. The prismatic points of the sphere move with the sphere, but background points are fixed. So, some of the background points near the prismatic points are added or removed when sphere is moved, and the connectivity of the point whose surrounding points are changed should be newly obtained. The speed of the sphere is $M_{sphere} = 0.5$ and free stream Mach number is $M_\infty = 1.5$. So, the relative free stream Mach number of sphere is 2. The reference case is stationary sphere problem with $M_\infty = 2$. The spatial discretization scheme is GC-LSM with AUSMPW+ and the time integration scheme is LU-SGS with dual time-stepping.

Fig. (11) shows the comparison of the pressure field between the test case and reference. From the obtained numerical results, it seems that both results are almost same although the nodes distribution are different because speed of each sphere is different. To confirm this in detail, Fig. (12) shows the pressure coefficient distribution along stagnation line and surface. It can be also seen that the pressure distribution including shock profile are very similar to the reference. Thus, this results presented here may show development possibility of the meshless method in supersonic or hypersonic flows on complex geometry.

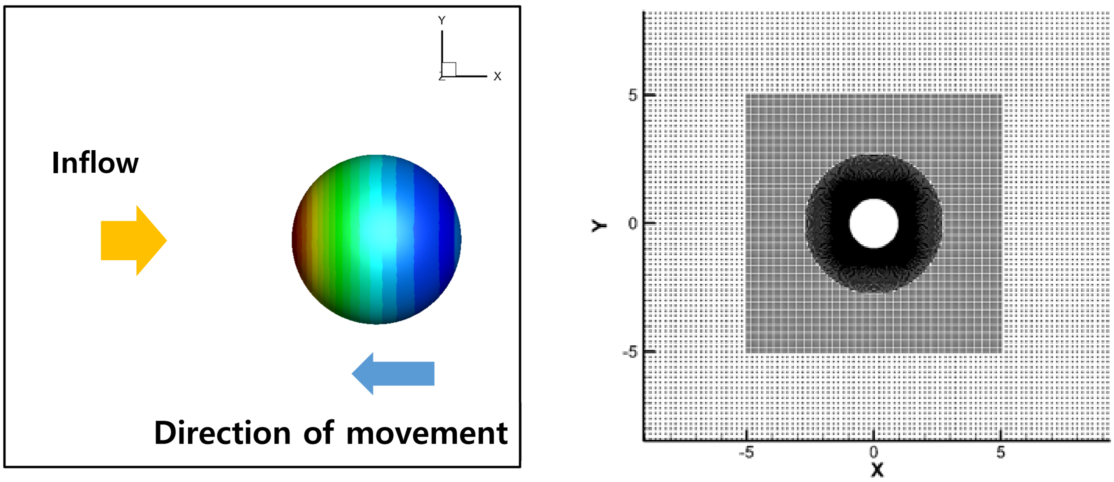

Figure 10: node distribution around sphere

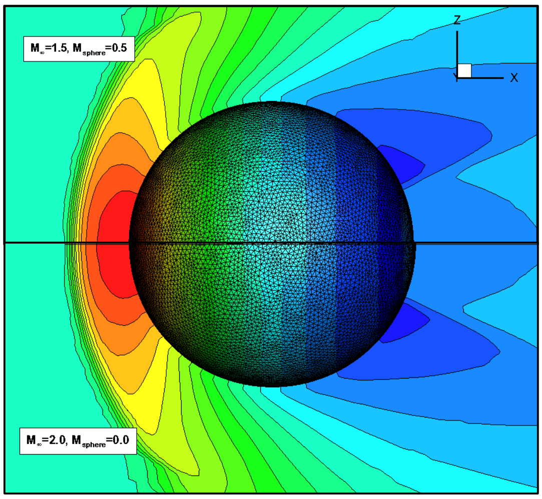

Figure 11: pressure contours

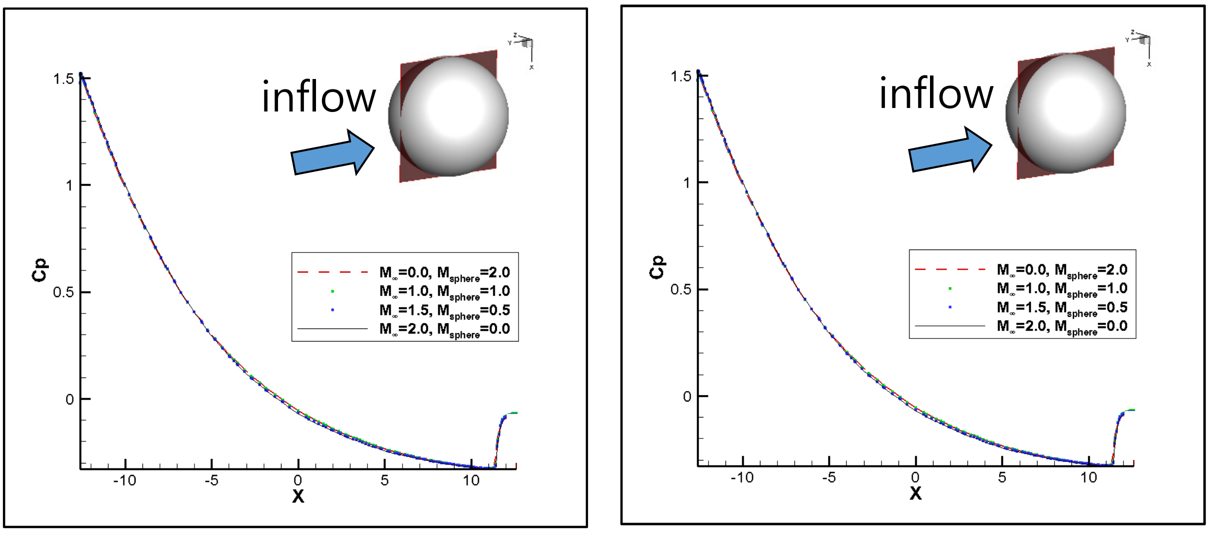

Figure 12: pressure distribution along stagnation line and surface

6 Conclusion and Future Work

In this study, Least Squares Method with Geometric Conservation Law(GC-LSM) is developed to analyze compressible flow robustly and accurately even when strong shock exists. The method of Lagrange multiplier was used to satisfy geometry conservation law and 1^{st} order consistency to least squares method. AUSMPW+ scheme which can compute accurately in hypersonic flows, and LU-SGS for implicit time integration are applied to the Meshless method. Numerical experiments show that the developed method gives improvements on accuracy and robustness in compressible flows with strong shock according to the comparison analyses of the numerical results with the original version of Least Squares Method.

Acknowledgments

- This research was supported by Space Core Technology Program through the National Research Foundation of Korea(NRF) funded by the Ministry of Science, ICT & Future Planning(NRF-2015M1A3A3A05027630)
- This work was supported by the Brain Korea 21 Plus Project in 2016

References

[1] G. R. Liu. *Mesh Free Methods: Moving Beyond the Finite Element Method*. CRC Press, 2003.
[2] D. Sridar and N. Balakrishnan. An upwind finite difference scheme for meshless solvers. Journal of Computational Physics. 189: 1-29, 2003.
[3] A. Katz and A. Jameson. A Comparison of Various Meshless Schemes Within a Unified Algorithm. AIAA 2009-596, 47th AIAA Aerospace Sciences Meeting Including The New Horizons Forum and Aerospace Exposition, Orlando, Florida, 2009.
[4] J. Huh, K. Kim and S. Jung. Meshless Method for Simulation of 2-D Compressible Flow. The 2013 Asia-Pacific International Symposium on Aerospace Technology, Takamatsu, Japan, 2013.
[5] K. Kim, C. Kim and O. Rho. Methods for the Accurate Computations of Hypersonic Flows I. AUSMPW+ Scheme, Journal of Computational Physics, 174: 38-80, 2001.
[6] D. Shepard. A two-dimensional function for irregularly spaced points. Proceedings of the 23rd ACM National Conference, 517-524, 1968.
[7] P. Lancaster and K. Salkauskas. Surfaces generated by moving least squares methods. Math. Comput. 37: 141–158, 1981.
[8] A. Jameson. Analysis and Design of Numerical Schemes for Gas Dynamics 1 Artificial Diffusion, Upwind Biasing, Limiters and Their Effect on Accuracy and Multigrid Convergence. International Journal of Computational Fluid Dynamics, 4:171-218, 1995.
[9] S. Yoon and A. Jameson. Lower-Upper Symmetric-Gauss-Seidel Method for the Euler and Navier-Stokes Equations, AIAA Journal, 26(9): 1025-1026, 1988.
[10] H. Q. Chen and C. Shu. An Efficient Implicit Mesh-Free Method To Solve Two-Dimensional Compressible Euler Equations. International Journal of Modern Physics C., 16(3): 439-454, 2005.
[11] J. Rhee, J. Huh, K. Kim and S. Jung. Three dimensional meshless point generation technique for complex geometry. The 2015 World Congress on Aeronautics, Nano, Bio, Robotics, and Energy, Incheon, Korea, 2015.